



Improved corrosion and wear protection performance of St12 steel by Ni-Cr-Al oxide coating

Hurieh Mohammadzadeh^{a,*}, Robabeh Jafari^b, Artin Azarگون^c

^{a*} Associate professor, Department of Materials Science and Engineering, Faculty of Engineering, Urmia University, Urmia, Iran.

^b Assistant professor, Department of Materials Science and Engineering, Faculty of Engineering, Urmia University, Urmia, Iran.

^c Bachelor Graduated, Department of Materials Science and Engineering, Faculty of Engineering, Urmia University, Urmia, Iran.

Received: 19 November 2024; Accepted: 8 June 2025

*Corresponding author, E-mail: h.mohammadzadeh@urmia.ac.ir

ABSTRACT

Metal oxides have a wide industrial application and are an important component of engineered nanocomposites that can improve the surface properties of metals by applying them to a variety of substrates through coating methods. In the present study, the Ni-Cr nano-oxide ($\text{NiO/NiCr}_2\text{O}_4$) was synthesized by co-precipitation to increase the durability of St12 carbon steel in harsh environments against corrosive and abrasive materials. Subsequently, the surface of St12 carbon steel sheets was coated by electrophoretic deposition (EPD) at 110V-3min. The properties of the synthesized nanocomposite and coatings were investigated by XRD, FTIR, FESEM and optical microscope (OM). The results showed that NiO and NiCr_2O_4 form nanoscale deposits with a crystallite size of 28.8nm and an average particle size of 60-80nm. The wear and corrosion behavior of the St12 substrate and coatings was investigated using ball-on-disk wear, EIS and polarization tests. XRD analysis of the coating materials after sintering revealed Ni, NiCr_2O_4 and phases of NiAl_2O_4 and Al formed during sintering as a result of Al addition. The results showed that the Ni-Cr oxide nanocomposite was successfully deposited on the St12 surface by EPD. The average coating thickness was measured to be 10.76 μm . The improvement in wear behavior was determined by measuring 1.8 and 2.1 mg mass of worn material for the coated sample and substrate, respectively. According to the Tafel analysis, the corrosion current density (i_{corr}) was 10.3 and 140.3 $\mu\text{A}\cdot\text{cm}^{-2}$ for the prepared coating and substrate, respectively, showing the considerable evolution of the corrosion behavior of bare steel by adding coatings up to 13 times. The electrochemical impedance spectroscopy (EIS) data were used to evaluate the corrosion mechanism and simulate the corresponding electrical equilibrium circuit. The charge transfer resistance (R_{ct}) was 7934.6 and 134.49 Ω for the coated sample and the bare St12 substrate, respectively.

Keywords: $\text{NiCr}_2\text{O}_4/\text{Ni-Al}$ spinel oxide; Coating; Electrophoretic deposition (EPD); Wear; Corrosion; Nano composite.

1. Introduction

The accelerated growth of the flexible and sustainable materials industry has led to the development of new materials and composite structures. The concept of nanomaterials and nanocomposites in materials has evolved to increase the quality of products and their durability. Nowadays, nanocomposites are widely developed and used in various industries, such as aerospace, electronics, micro- and nanomechanics,

and biomaterials [1,2]. The surface of materials in various industrial applications is exposed to various mechanical, physical and chemical attacks and damages. Accordingly, metal oxide nanocomposites could protect the surface when applied as coatings on the material surface [3,4].

Among various metal oxides, nickel and chromium oxide nanoparticles exhibit some outstanding electrochromic, mechanical and physical properties, such as wear resistance,

corrosion resistance, high durability in various environmental and operating conditions [4,5]. Due to the high electrochemical resistance of Ni and Cr oxides, they are excellent candidates for coatings applied to susceptible materials under corrosive conditions [6]. In addition, the possible reaction between NiO and Cr_2O_3 under the desired thermal conditions can produce NiCr_2O_4 , a spinel with antibacterial and lubricating properties [7]. This spinel, NiO and Cr_2O_3 have very good stability at high temperatures [8]. Metal oxide nanocomposites can be produced by various methods, including combustion methods [9], mechanical alloying [10], microwave [11], chemical co-precipitation [12], high energy ball-milling [13]. However, chemical coprecipitation is a simple and inexpensive method commonly used by researchers to produce oxide nanocomposites with excellent purity and very fine particle size [14].

Singh et al. applied [15] Ni/ Al_2O_3 and Ni/ Cr_2O_3 nanocomposite coatings to carbon steel pipes used in high-voltage transmission lines to improve the resistance to erosive wear. The results showed that the Ni/ Cr_2O_3 coating offered superior performance compared to its Ni/ Al_2O_3 counterpart. Wang et al. [16] presented in their study that a Ni-WC-Co nanocomposite coating applied to the surface of stainless steel by electrophoretic deposition significantly improved the wear behavior and hardness of the substrate. Abdel Halim et al. discussed that Sn-NiO-ZnO nanocomposite coating was applied on steel carbon to improve the corrosion behavior of steel [17]. Ryu et al [18] coated the steel substrate with GO nanosheets using EPD. They reported that the coated steel surface exhibited significantly better corrosion resistance compared to bare steel. Heidari et al. [19] investigated the deposition of nano-SiC nickel composite coatings on St12 steel using the electrodeposition method. Their results showed that these coatings significantly improve wear resistance, corrosion resistance and surface hardness compared to pure nickel coatings. These improvements offer significant benefits for industrial applications, particularly in improving the performance of St12 steel. Such nanocomposite coatings can be deposited on carbon steels by various methods, including sol-gel [20], CVD [21], PVD [22], electro-plating [23], pyrolysis spray [24] and electrophoretic deposition [25]. Electrophoretic deposition (EPD) is a coating method for depositing various types of metallic and non-metallic materials (especially for coatings of ceramics and composites) in powder form and is therefore often used as a versatile, popular and cost-effective approach. In EPD, the coating materials in charged powder form are suspended in the electrolyte and form a stable suspension

that migrates due to the strong electric field and deposits on the oppositely charged electrode [26].

In this study, the Ni-Cr spinel oxide was synthesized using the co-precipitation method, followed by the deposition of the Ni-Cr spinel and alumina nanocomposite coating on St12 steel sheets using the electrophoretic deposition (EPD) technique. The mechanical, morphological and corrosive properties of the coated and uncoated St12 steel were comprehensively evaluated. This work highlights the effective application of the EPD process to produce an effective coating. Furthermore, a chemical interaction during the sintering process between the Al additive and NiO led to the formation of NiAl_2O_4 , which contributed to the improved performance of the coating alongside the NiCr_2O_4 phase. The nanocomposite coating showed significant improvements in both corrosion resistance and mechanical properties, demonstrating its potential for advanced protection applications.

2. Experimental

The Ni-Cr spinel oxide-based nanocomposite with 50wt% NiO-50wt% Cr_2O_3 was synthesized from nickel and Chromium salts of $\text{NiSO}_4 \cdot 6\text{H}_2\text{O}$ and $\text{Cr}_2\text{Na}_2\text{O}_7 \cdot 2\text{H}_2\text{O}$ (Merck, Germany, purity $\geq 99\%$) through co-precipitation approach [4]. The appropriate amounts of nickel and chromium salts were determined to achieve a 50% NiO - 50% Cr_2O_3 stoichiometry after synthesis. Then, the salts' each were dissolved separately in 100 ml distilled water using stirrer. After completely liquidation of salts, they were added to a beaker and stirred until a uniform solution was achieved, the pH value was observed 3.8 after solutions uniformity. By heating the solution temperature was set at 78 °C then the pH mixture gradually increased to 10 by adding dropwise NH_3 solution. Then stirring process at 78 °C continued until pH decreased to 7 (for 5 hours). After a while, the precipitation of the material appeared, sediments collected from solution through filter paper washed several times by distilled water and ethanol. Now filters were used in each washing stage. Eventually the produced material was dried at the oven 80 °C for 2 hours. Then, it was calcined at 720 °C for 1 hour (Figure 1).

Al nano powder (Sigma-Aldrich, USA, 99.9%, <100nm), 1-Butanol organic solvent ($\text{C}_4\text{H}_{10}\text{O}$, Merck, Germany, purity $\geq 99.5\%$) and iodine (I_2 , Merck, Germany, 99.9%) were employed for EPD. The substrates were St12 sheets of 3×3 mm². The substrate sheets were sandblasted at 6 bar. The substrates were cleaned by remaining in alkaline solution (NaOH 10%) at 60 °C for 15 min, then bare samples were washed with acetone ($\text{C}_3\text{H}_6\text{O}$, Merck, Germany, purity $\geq 99\%$) in the ultrasonic

bath for 15 min followed by distilled water.

The zeta potential data collected showed that the iodine concentration of 0.6 g/L had the highest value of 40.1 mV, compared to 0.4 and 0.8 g/L, which were 27.6 and 23.4, respectively. Therefore, 0.6 g/L was chosen as an appropriate amount of dispersant. The dispersant in the amount of 0.6 g/L iodine was prepared and added to the organic solvent butanol and stirred for 1 hour. Then 6 g/L Ni-Cr oxide nanopowder was added to the solution. After 2 hours of mixing, 0.6 g/L nano-Al powder was mixed with the solution as a dispersant and then stirred for 24 hours. Finally, the suspension bath was dispersed for 5 minutes using an ultrasonic vibration probe (Figure 1).

Ni-Cr oxide nanocomposite was coated on St12 substrates by direct current (DC) cathodic EPD process. St12 plates were used as anodic and cathodic electrodes that were placed in the coating electrolyte bath parallel to each other at a distance of 1 cm. The coating voltage and the coating time were set to 110 V and 3 minutes respectively. After the coating process, the samples were oven-dried at 110 °C for 2 hours and then sintered at 750 °C for 2 hours (in the Ar-Flow atmosphere, 99.999 %).

Zeta potential analysis (SZ-100, HORIBA, Ltd., Japan) was conducted to determine the appropriate amount of iodine dispersant used in the suspension preparation.

The morphology and the thickness of the coating was evaluated by an optical microscope

(OM, Optika B-383Pli, Italy) and a field emission scanning electron microscope (FE-SEM TESCAN MIRA3, Czech Republic).

The chemical properties of the synthesized powder were investigated by Fourier transform infrared spectroscopy (FTIR, Thermo-AVATAR, USA, wavenumber 400–4000 cm^{-1}) and X-ray diffraction analysis (XRD Philips PW1730, Netherlands) with Cu K α radiation ($\lambda = 1.540598 \text{ \AA}$). The 2θ range for the analysis was 10° – 80° , with a step size of 0.05° and a measurement time of 1 second per step. The device was operated at 40 kV and 30 mA. A Vickers microhardness tester (HV-1000Z, PACE Technologies, USA, and a load of 1 g, 15 s long) was used to determine the hardness of the coating and the bare substrate. The average of the results of 15 indentations was reported as the microhardness of the samples.

The coefficient of friction and wear properties of the Ni-Cr oxide nanocomposite coatings were evaluated by the ball-on-disk test according to the ASTM G99 standard at ambient conditions. A steel ball (52100 AISI, 55-60 HRC, main diameter = 6 mm, tip diameter = 3 mm) rotated on the samples under a normal load of 6 N at ambient temperature. The rotation speed and total sliding distance were 200 rpm and 120 m respectively.

Electrochemical polarization (Galvanostatic device, OrigaFlex 01A, OrigaLys ElectroChem SAS, France) and electrochemical impedance spectroscopy (EIS, at a frequency of 10mHz-

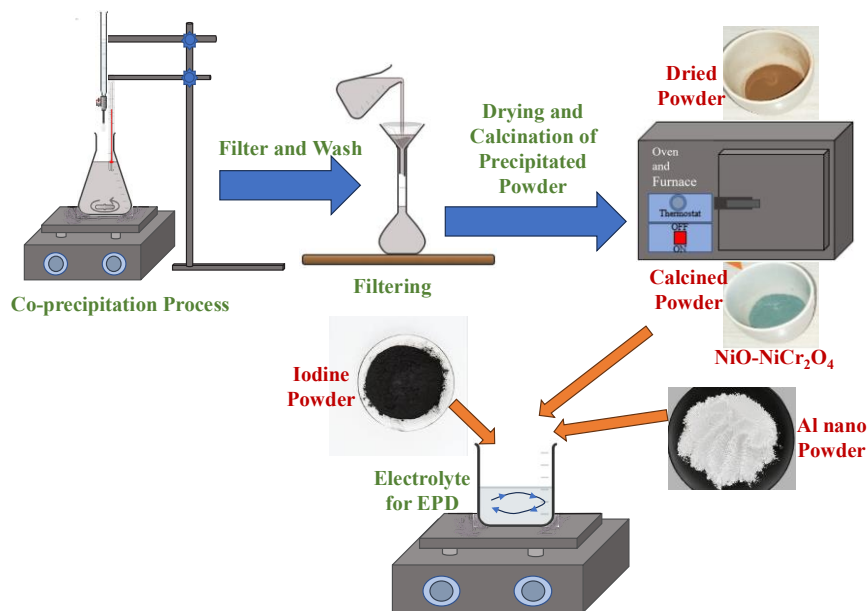


Fig. 1- Schematic illustration of nano-composite and the electrolyte preparation.

100kHz, using a sinusoidal voltage with an amplitude of 10 mV) were used to study the corrosion behavior of the substrate and coating in the 3.5% NaCl standard solution in the working environment. The speed of voltage scanning was 1 mV/s in the range of -1 to 1.5 V. The working, counter and reference electrodes were respectively the substrate/coated sample, platinum and calomel. Before analysis, the coated sample and the substrate were equilibrated in the electrolyte for 1 hour, and the open circuit potential was measured after 20 minutes. After polarization and EIS analysis, the corrosion data were evaluated using Tafel extrapolation and Zview software.

3. Results and Discussion

3.1. Ni/Cr nano-oxide composite

The results of the XRD pattern and the FTIR

spectrum of the calcined Ni/Cr nanooxide powder are shown in Figure 2. Figure 2a shows the presence of NiO (JCPDS card number 04-0835) and spinel NiCr₂O₄ (JCPDS card number 89-6615) in the synthesized product. According to the literature, calcination of Ni/Cr nanooxide at 700 °C yields a stable NiCr₂O₄ spinel with cubic structure and main plane indices (211), (220), (224) and (113) [33]. The crystallite size was calculated to be 28.8 nm (Equation 1 [30]),], Debye-Scherrer; D, κ, β, λ, and θ are the crystallite size, constant number, most abundant (0.94), full width at half maximum (FWHM), wavelength, and X-ray diffraction angle for high-intensity Bragg peaks, respectively.

$$D = \frac{k\lambda}{\beta \cos \theta} \quad (1)$$

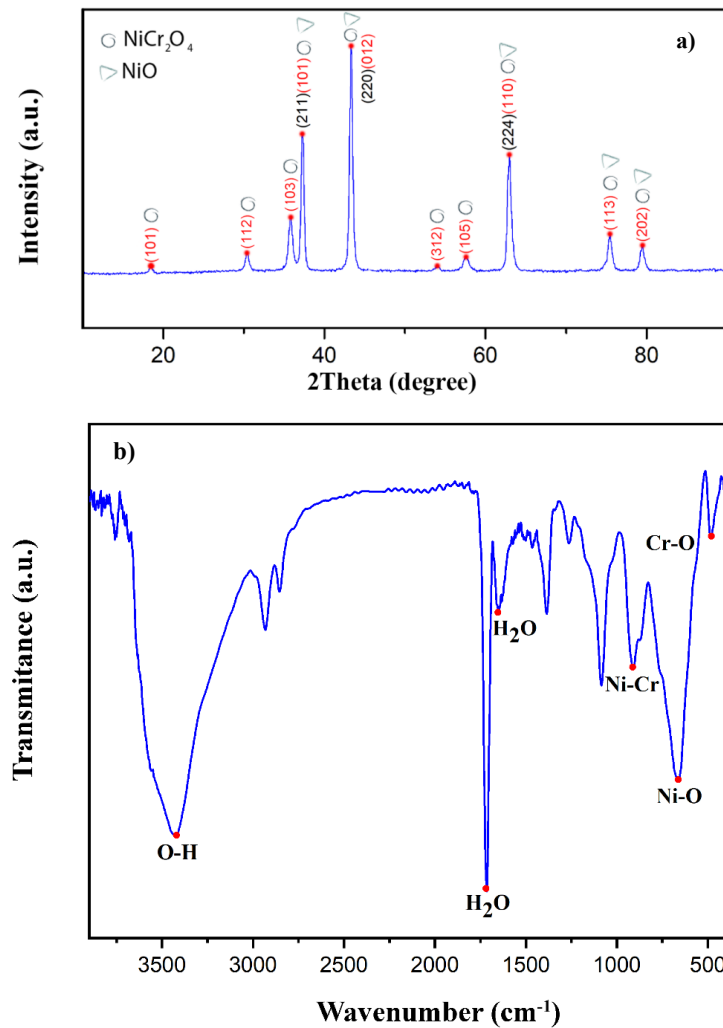


Fig. 2- a) XRD pattern and b) FTIR spectrum of the synthesized nanocomposite of Ni-Cr oxide after drying and calcination.

Figure 2b shows the chemical composition of the elements involved and their chemical bonds. The peak at wavenumber 3431 cm^{-1} refers to the O-H stretching vibrational bond [31]. The peaks at 1575 and 1417 cm^{-1} show the bonding of water molecules (H_2O) with bending vibration [32]. In addition, the occurrence at 925 cm^{-1} shows the stretching vibration of Ni-Cr metal-metal bonding [33]. The stretching vibrations of Cr-O and Ni-O in the interstitial sites of the cubic crystal appear at 493 and 612 cm^{-1} [34]. These results confirm the formation of the NiO and NiCr_2O_4 nanocomposite after calcination of the co-precipitated powder.

Figure 3a and b present the FESEM images of the co-precipitated Ni/Cr nano-oxide composite powder after calcination to study the morphology and size of the particles. FESEM images of nano powders presents that the particles are spherical with nano size. Some agglomerates (Figure 3b; with average size of 1.2 μm) are formed due to the intrinsic attraction between nano-particles. According to Figure 3a, the particle size is among 60-80 nm.

3.2. Ni-Cr oxide nanocomposite coatings

3.2.1. Morphology of coating

Ni/Cr nano-oxide/nano-Al particles were deposited on the St12 substrate using EPD. Figure 4a and b show the optical microscope (OM) images of the applied coating and the corresponding cross-section. According to Figure 4a, the coating covered the surface evenly. However, some narrow cracks and porosities were observed on the coating, which may form during the drying step due to the removal of volatiles from the coating material. In Figure 4b, the cross-section of the coating has an average value of 10.76 μm , which results from almost 15 measurements at different locations on the coating. The XRD pattern of the coating from the sintered coated sample is shown in Figure 4c, which shows Ni (JCPDS 96-901-3004), Al (JCPDS

00-004-0787), NiCr_2O_4 (JCPDS 00-023-0432) and NiAl_2O_4 (JCPDS 00-010-0339). The NiCr_2O_4 spinel with a cubic crystal structure is a stable phase that remained in the coating after sintering. However, the formation of ceramic NiAl_2O_4 and metallic Ni phases by the Al addition has occurred after sintering by the chemical reaction of Equation 2 [35]. The O_2 molecules trapped between the coating material during deposition must have contributed to this reaction as sintering took place in a neutral gas stream. The accessible surface of the NiO particles can serve as a source of O_2 through a diffusion mechanism.

Figure 5 shows the FESEM images of the coating surface after sintering. Figure 5a and b show the morphology of the coating surface in two magnifications. Figure 5c and d show the FESEM image and the corresponding element map of the coating, which shows a uniform distribution of the elements (Cr, O and Ni). The colors red, green, blue and yellow represent Cr, Al, O and Ni, respectively. There are local concentrations of Al. Such Al aggregations could occur during sintering at 750°C due to the melting of Al and its accumulation due to the increased capillary force between the large surface areas between the nanoparticles of the coating. In Figure 5b, the particles that make up the coating consist of spherical and quasi-spherical particles with a relatively uniform size distribution, similar to the original Ni/Cr nano-oxide powder (Figure 3a). The EPD coating method does not form a smooth coating due to the influential parameters such as the generated electric field, particle size and their tendency to sediment in suspension. These are characteristics of the electrochemical coating process that do not ensure compaction of the sedimented material on the surface during deposition, which leads to the formation of porosities in the coating structure (Figure 5a).

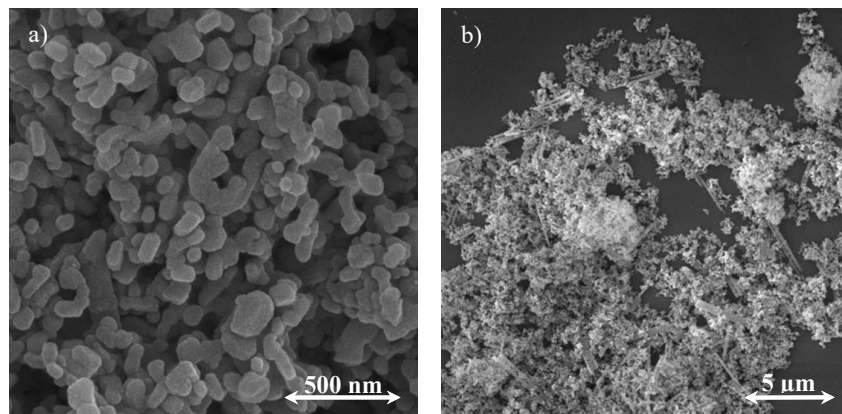


Fig. 3- FESEM, images of the synthesized nanocomposite after drying and calcination.

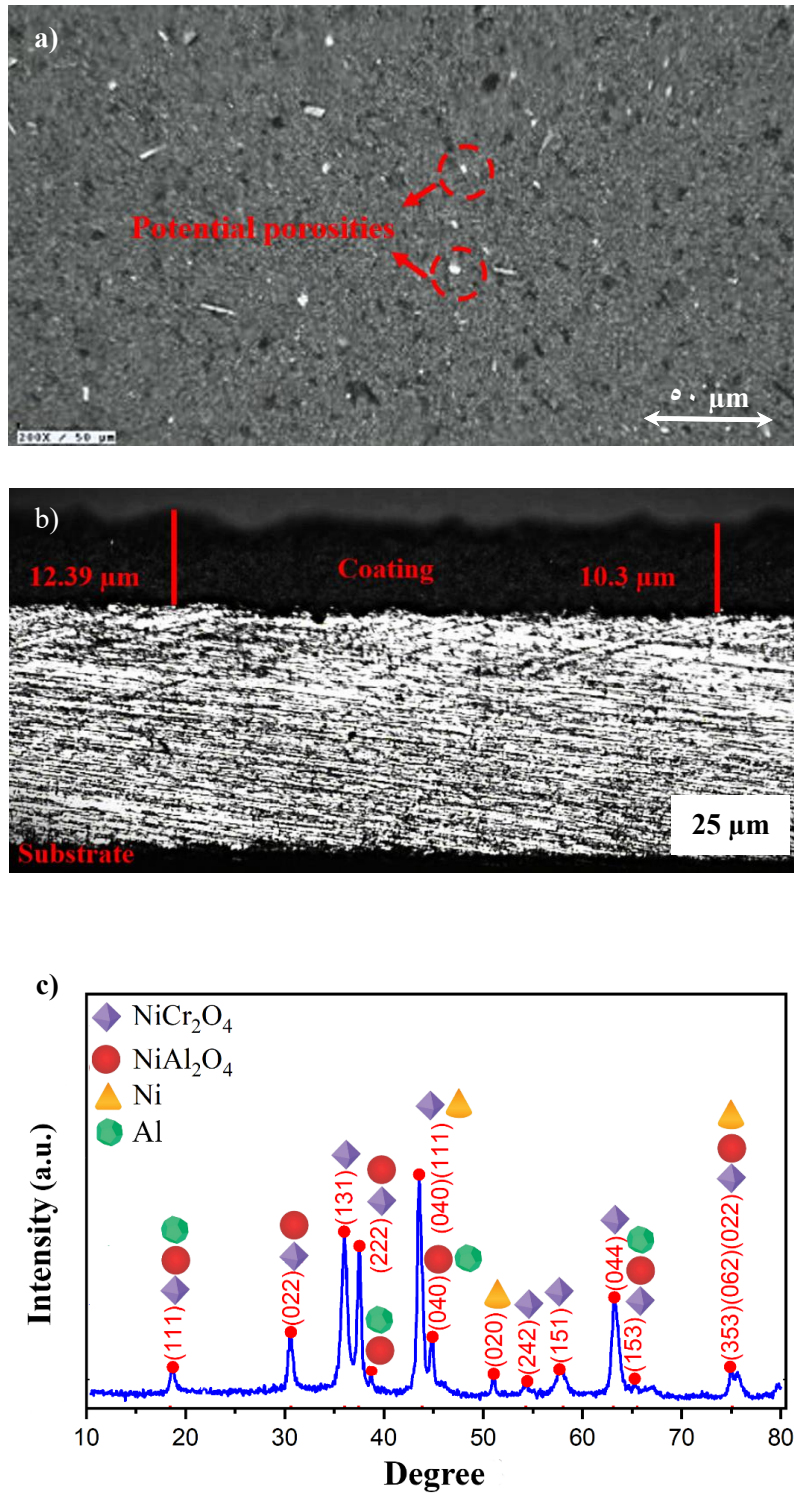


Fig. 4- Optical microscope (OM) images of coated sample form a) surface and b) cross section and c) XRD pattern of the coating after sintering.

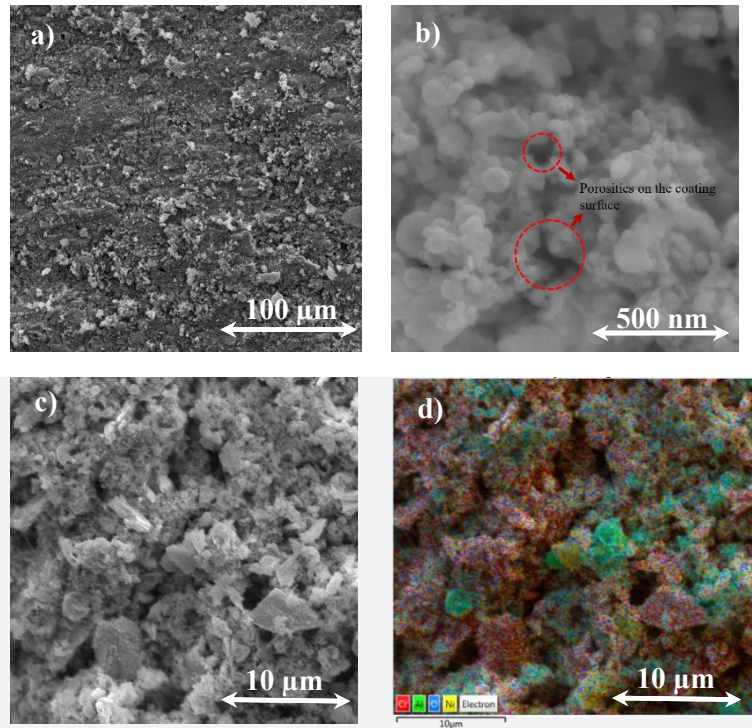


Fig. 5- FESEM images and the elemental maps of the coating; Yellow, green, purple and red collors are for Cr, O, Al and Ni, respectively.

3.2.2. Wear and microhardness of coating and substrate

The mechanical properties of the St12 substrate and the coated sample were evaluated by ball-on-disk wear and the Vickers microhardness test at room temperature. The results of the wear analysis are shown in Figures 5a to d. The worn mass is defined by the weight loss caused by the perpendicular force on the moving surface over the distance traveled [36].

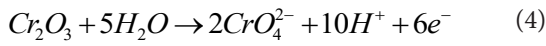
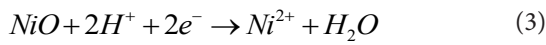
Figure 6a and b are OM images of the worn surface. The average values of the width of the worn track were measured to be 167.4 and 93.9 μm for the St12 substrate and the coated sample, respectively. This shows that the sliding ball abraded the surface less on the coated sample than on the bare substrate. Figure 6c shows that the friction coefficient curve for the coated sample is lower than that of the bare substrate. This indicates which both the wear and the coefficient of friction were improved, which can be attributed to the presence of a laminate-structured $\text{NiO/NiCr}_2\text{O}_4$ spinel-based oxide nanocomposite with self-lubricating properties that prevented excessive degradation of the coating. The values of mass loss and friction coefficient during the 120 m sliding of the grinding ball over the bare substrate and the coating

samples are shown in Figure 6d. The worn mass and coefficient of friction decreased by 15 % and 13 %, respectively, which can be attributed to the additional plasticity of the NiCr_2O_4 nanocomposite layer structure in the coating [37-39]. The lower coefficient of friction shows that the grinding ball can be moved more easily on the coating than on the bare substrate. The nanocomposite coating based on $\text{Ni-NiCr}_2\text{O}_4/\text{Ni-Al}$ spinel oxide significantly improved the wear resistance of the St12 surface. The hard ceramic NiCr_2O_4 and NiAl_2O_4 phases are the reinforcing materials in the applied coating. The Vickers microhardness of the substrate and coating was measured at a minimum of 15 points and the average values were calculated to be 107.3 and 204.1 Hv respectively. This confirms the significant improvement in surface hardness due to the porous coating created. The improved hardness is due to the presence of tough spinel with unique structures (NiCr_2O_4 , NiAl_2O_4), which led to an improvement in the wear properties of the coated sample.

3.2.3. The corrosion behavior

In order to evaluate the behavior of the samples in the corrosive environment, potentiostatic polarization analysis was performed in a 3.5 % NaCl solution for the bare St12 sheets and the

samples coated with a Ni-NiCr₂O₄/Ni-Al spinel oxide-based nanocomposite from a stabilized state of the open circuit potential of the electrode. Figure 7a shows the Tafel curves of the samples as a function of potential and current density. Using the Tafel extrapolation method, the corrosion parameters such as the corrosion potential and current density can be determined, which are shown in Table 1. Note that the values β_a and β_c were calculated from the slopes of the anodic and cathodic branches of the Tafel curves. Relevant possible reactions at the interfaces between coating and solution that may take place during corrosion analysis were mentioned in the same order as below [4] by reactions 3, 4 and 5.



The collected information from Tafel chart of the coated and uncoated sample clearly shows that the precipitated nanocomposite coating improves the corrosion behavior of the substrate by acting as an appropriate barrier against the corrosive environment. This may be due to the complex trajectories created by the nanoparticles

(connected and unconnected porosities created during the deposition process in suspension as well as during drying), which cause the electrolyte to deviate from the direct path and disperse in the coating. Compared to bare steel, the ceramic nanocomposites are less susceptible to interaction with the surrounding atmosphere, which is also reflected in the development of the corrosion properties, which are described by the corrosion potential on the vertical axis of the Tafel plot (E_{corr}). The more positive (E_{corr}), the better the corrosion resistance [40]. The thickness of the coating is another influential factor that protects the steel surface. An increase in coating thickness means that the corrosive agents have a longer path to breakthrough, which reduces the corrosion rate. In agreement with the results of Tafel and EIS, 10.76 μm was sufficient to achieve useful corrosion resistance.

The results of EIS analysis can provide more details about the electrochemical interactions between samples and corrosive substances. The alternating current in the chemical cell containing the samples as electrodes provides the frequency and impedance (the imaginary and real impedance) to extract the Nyquist, bode-phase angle and impedance modulus plots [41], which are shown in Figure 7b to d for the bare St12 substrate and the coated sample, respectively.

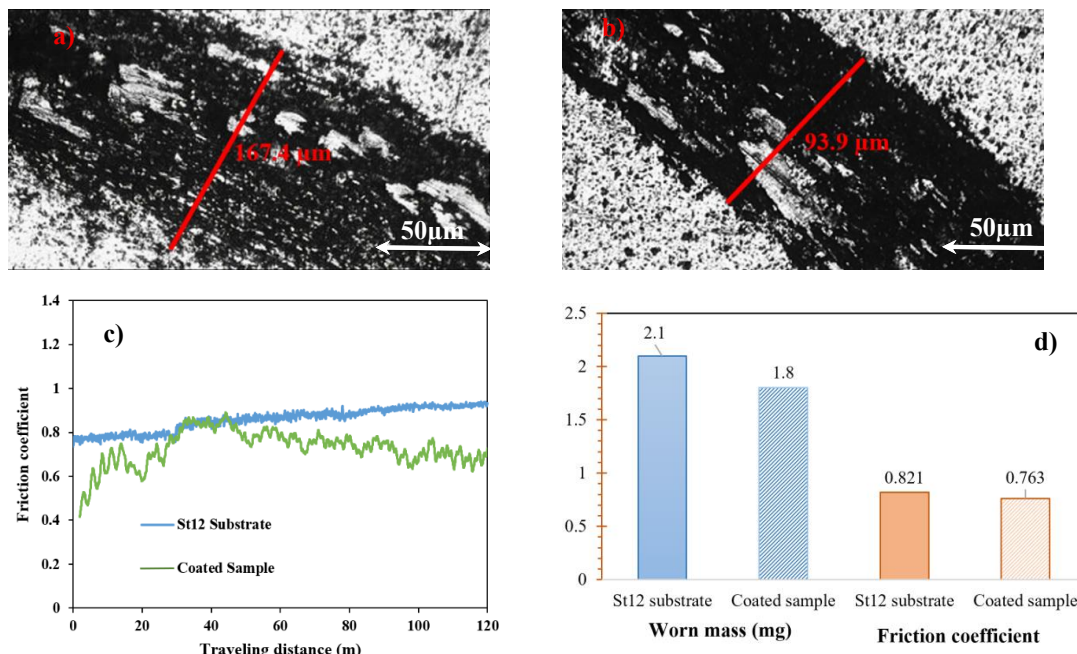


Fig. 5- Wear results of the St12 substrate and the coated material; a) OM image of the worn St12 substrate, b) OM image of the Worn coated sample, c) the friction coefficient curve verse wear distance and d) the values of worn mass and friction coefficient.

The semicircles in the Nyquist plot in Figure 7b show the interfaces between the electrolyte and the sample. The total value of the diameters of the semicircles is the resistance of the material to corrosion [42]. Although the number of semicircles in the Nyquist diagram is 2 for both the substrate and the coated sample, the bare substrate showed a reversed tail (induction loop). The induction loop at low frequencies shows the penetration of the electrolyte into the surface and its reaction with the substrate, indicating the sensitivity of the sample to pitting [43]. In the Nyquist diagrams of the coated sample and the bare St12, two capacitance

semicircles can be seen, which are related to the interfaces between the electrolyte coating/corrosion product layer and the electrolyte substrate. Figure 7c shows the modulus plot of the body impedance of the uncoated substrate (St12) and the sample coated with the Ni-NiCr₂O₄/Ni-Al spinel nanocomposite. The value of the impedance at low frequencies represents the corrosion resistance in the electrolyte. The coated sample has the highest impedance at low frequencies (the diameter of the semicircle) and therefore has better corrosion resistance. The node-phase-angle diagrams in Figure 7d show some peaks due to the capacitance

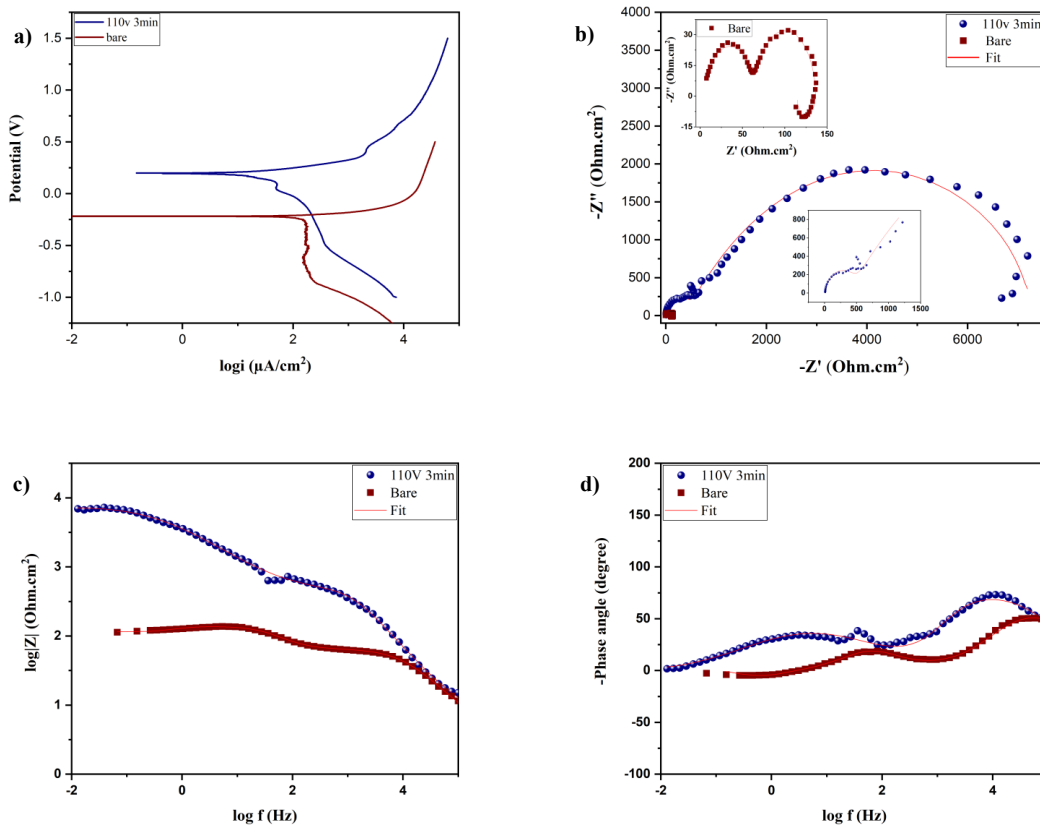


Fig. 7- a) The polarization curves of bare and coated, EIS curves of the coated samples, b) Nyquist plot; c) bode-impedance modulus, d) bode-phase angle plot of the bare and coated sample.

Table 1- The corrosion parameters for bare and coated sample achieved from the Tafel polarization analysis

Samples	β_a (mV/dec)	β_c (mV/dec)	E_{corr} (mV)	$i_{corr} \times 10^{-6}$ (A·cm ⁻²)
Coated sample	303	-343.8	197.3	10.3
Bare	200	-1277	-219	140.3

and resistance performance of the electrochemical elements simulated in the corresponding electrical equivalent circuit [44].

The EIS data can be quantified with the electrical data by describing them with a suitable electrical equivalent circuit. This was done for the present study using the ZView software and is shown in Figure 8a and b (for the bare St12 and the coated sample, respectively). The corresponding electrical data of the circuit elements are given in Table 2. R_s , R_c , R_p , R_{ct} and R_L are impedance values, while the resistance elements represent the electrolyte resistance, the pore resistance in the coating, the resistance of the iron oxide layer (passive layer) on the substrate, the charge transfer resistance and the resistance of the induction loop. The higher the value of $R_c+R_p+R_{ct}$, the better the corrosion resistance.

In Figure 8a and b, the capacitors are represented by CPE, including CPE_c , CPE_p and CPE_{dl} for the interfaces between coating and electrolyte, coating and passive layer, and passive layer and substrate. Due to the surface roughness of the samples, the capacitors are not ideal (constant phase element).

The capacitors form loops in the Nyquist diagram by forming loops with a semicircular shape [42]. Another electric element is the inductance L , which was observed in the equilibrium circuit of the bare substrate St12.

Figure 8c shows a schematic configuration of the coated sample in the corrosive environment based on the EIS results and the associated electrical equivalent circuit. The interactions between the corrosive substances in the electrolyte and the sample are shown in the figure as an electrical equivalent circuit diagram. In addition, the microcracks in the coating material which penetrate deep enough into the substrate allow the electrolyte to reach the substrate and cause the metal substrate to interact and corrode with the O , OH and Cl ions of the electrolyte. The corresponding electrical equivalent circuit diagram is shown at the interface between the substrate and the coating (white circle). Due to the good protective effect of the coating, the corrosion activity at the interface between substrate and coating was low (R_{ct} was 73.89 compared to 7533 Ω for the bare St12).

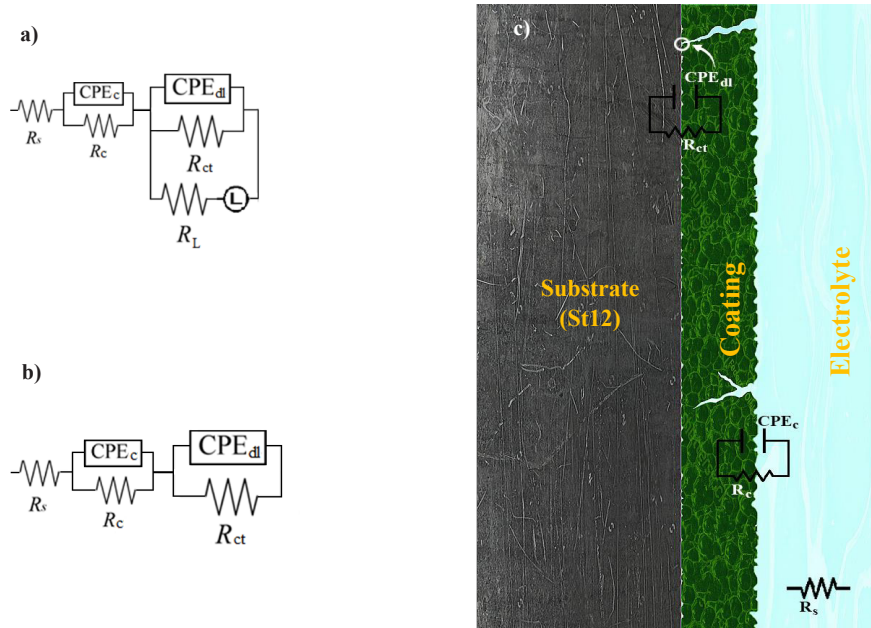


Fig. 8- Equivalent electrical circuits for a) the bare St12 substrate and b) the coated sample and c) the schematic configuration of the coated sample in the electrolyte.

Table 2- The fitting parameters obtained from simulating the EIS data in the attributed electrical equivalent circuits

Sample	R_s (Ω)	$Y0_p$ ($S.sec^n.cm^{-2}$)	n_p	R_p (Ω)	$Y0_{dl}$ ($S.sec^n.cm^{-2}$)	n_{dl}	R_{ct} (Ω)	R_L (Ω)	L (Henri. cm^2)
110V 3min	5.89	4.38E-07	0.96	401.6	7.02E-05	0.60	7533		
Bare	3.99	1.31E-6	0.85	60.6	8.95E-5	0.90	73.89	163.1	43.75

4. Conclusions

In the present study, a Ni-Cr oxide nanocomposite was synthesized by chemical coprecipitation. This nanocomposite and nano-Al powder were applied to the surface of carbon steel (St12) by EPD. The properties of the produced coatings, including mechanical, electrochemical and morphological properties, were investigated. The results showed that:

1- According to the FTIR and XRD data, the prepared nanocomposite powder consisted of NiO and cubic spinel NiCr_2O_4 with an average crystallite and particle size of 28.8 nm and 60-80 nm, respectively.

2- The nanocomposite of Ni, Al, NiAl_2O_4 and NiCr_2O_4 coating formed after sintering. Although Ni, O and Cr were still uniformly distributed in the coating, Al showed localized concentrations.

3- The coating significantly improved wear resistance, microhardness and corrosion resistance. The microhardness values were 107.3 and 204.1 Hv for the bare and coated samples, respectively.

4- The corrosion rates for bare and coated St12 steel were 10.3 and $140.3 \mu\text{A}\cdot\text{cm}^{-2}$, respectively. The highest and lowest corrosion resistance values were found to be 7934.6 and $134.49 \Omega\cdot\text{cm}$ for the coated sample and the bare St12 substrate respectively. Induction loop in the bare sample confirmed a weaker response to corrosive elements.

References

1. Y.S. Lo, C.C. Chang, P.C. Lin, S.P. Lin, C.L. Wang, Direct growth of structurally controllable hydroxyapatite coating on Ti-6Al-4V through a rapid hydrothermal synthesis, *Appl. Surf. Sci.* 556 (2021) 149672.
2. D.K. Rajak, D.D. Pagar, R. Kumar, C.I. Pruncu, Recent progress of reinforcement materials: A comprehensive overview of composite materials, *J. Mater. Res. Technol.* 8 (2019) 6354–6374.
3. M.L. Grilli, *Metal oxides*, Metals (Basel). 10 (2020) 1–3.
4. H. Mohammadzadeh, R. Jafari, A. Azargoon, Mechanical, morphological, and corrosion features of Ni-Cr oxide nanocomposite coating deposited on SS304 by EPD, *Int. J. Appl. Ceram. Technol.* (2024) 1–18.
5. Y. Zhu, Electrochromic and Electrochemical Energy Storage Properties of Micro-nano Hierarchical NiO film, *Int. J. Electrochem. Sci.* 14 (2019) 7401–7409.
6. J.R. Xavier, Electrochemical, mechanical and adhesive properties of surface modified NiO-epoxy nanocomposite coatings on mild steel, *Mater. Sci. Eng. B Solid-State Mater. Adv. Technol.* 260 (2020) 114639.
7. C. Ragupathi, V.T. Geetha, S. Narayanan, P. Tamizhdurai, G. Ramalingam, V.L. Mangesh, R. Kumaran, A.M. Alanazi, A.A.A. Bahajaj, M. Govindasamy, Study of Ce-doping effects on optical, morphological, magnetic, structural, and antibacterial properties of NiCr_2O_4 ceramics, *Mater. Sci. Eng. B Solid-State Mater. Adv. Technol.* 291 (2023).
8. M.G. Tsegay, H.G. Gebretinsae, G. G. Welegergs, M. Maaza, Z.Y. Nuru, Novel green synthesized Cr_2O_3 for selective solar absorber: Investigation of structural, morphological, chemical, and optical properties, *Sol. Energy.* 236 (2022) 308–319.
9. M.D. Lima, R. Bonadimann, M.J. de Andrade, J.C. Toniolo, C.P. Bergmann, Nanocrystalline Cr_2O_3 and amorphous Cr_2O_3 produced by solution combustion synthesis, *J. Eur. Ceram. Soc.* 26 (2006) 1213–1220.
10. S.M.H. Hoseini, M. Adeli, S.A. Hoseini, S.A. Hoseini, Facile synthesis of MgAl_2O_4 spinel matrix nanocomposite with TiC, AlTi_3 , and Al_2O_3 reinforcements by mechanical alloying, *J. Aust. Ceram. Soc.* 59 (2023) 269–280.
11. H.N. Deepak, K.S. Choudhari, S.A. Shivashankar, C. Santhosh, S.D. Kulkarni, Facile microwave-assisted synthesis of Cr_2O_3 nanoparticles with high near-infrared reflection for rooftop cooling applications, *J. Alloys Compd.* 785 (2019) 747–753.
12. H. Mohammadzadeh, H.R. Rezaie, M. Barati, D. Yu, H.R. Samim, Kinetics of nonisothermal reduction and carburization of WO_3 -NiO nano-composite powders by $\text{CO}-\text{CO}_2$, *Int. J. Chem. Kinet.* 51 (2019) 463–475.
13. M. Koroghli, V. Alimirzaloo, H. Mohammadzadeh, M. Kavanlouei, Sintering Behavior of WC-Co with Additives of TiC, VC, and (Ta, Nb)C: Microstructural and Mechanical Features, *J. Mater. Eng. Perform.* (2021).
14. M.A. Rahman, R. Radhakrishnan, R. Gopalakrishnan, Structural, optical, magnetic and antibacterial properties of Nd doped NiO nanoparticles prepared by co-precipitation method, *J. Alloys Compd.* 742 (2018) 421–429.
15. V. Singh, S. Kumar, D. Ratha, Synergistic effect of the addition of TiO₂ feedstock on solid particle erosion of Ni/Al₂O₃ and Ni/Cr₂O₃ coatings, *Wear.* 426–427 (2019) 250–257.
16. Y. Wang, Z. Xu, Nanostructured Ni-WC-Co composite coatings fabricated by electrophoretic deposition, *Surf. Coatings Technol.* 200 (2006) 3896–3902.
17. E.-S.M.S. 3 K. S. Abdel Halim 1, 2,* , Mohamed Ramadan 1, 2, K.M.H. 2, Tayyab Subhani 1, Enhancement of Surface and Interface Properties of Low Carbon Steel by Hybrid ZnO and NiO Nanoparticles Reinforced Tin Coating, *Crystals.* 12 (2022) 332.
18. S. Ryu, Y.J. Kwon, Y. Kim, J.U. Lee, Corrosion protection coating of three-dimensional metal structure by electrophoretic deposition of graphene oxide, *Mater. Chem. Phys.* 250 (2020) 123039.
19. G. Heidari, H. Tavakoli, S.M. Mousavi Khoie, Nano SiC-nickel composite coatings from a sulfamate bath using direct current and pulsed direct current, *J. Mater. Eng. Perform.* 19 (2010) 1183–1188.
20. H. Cheraghi, M. Shahmiri, Z. Sadeghian, Corrosion behavior of TiO₂-NiO nanocomposite thin films on AISI 316L stainless steel prepared by sol-gel method, *Thin Solid Films.* 522 (2012) 289–296.
21. A.M. Lazar, W.P. Yespica, S. Marcelin, N. Pèbère, D. Samélor, C. Tendero, C. Vahlas, Corrosion protection of 304L stainless steel by chemical vapor deposited alumina coatings, *Corros. Sci.* 81 (2014) 125–131.
22. A.B. Khelifa, S. Khamlich, Z.Y. Nuru, L. Kotsedi, A. Mebrahtu, M. Balgouthi, A.A. Guizani, W. Dimassi, M. Maaza, Growth and characterization of spectrally selective $\text{Cr}_2\text{O}_3/\text{Cr}/\text{Cr}_2\text{O}_3$ multilayered solar absorber by e-beam evaporation, *J. Alloys Compd.* 734 (2018) 204–209.
23. I.U. Haq, K. Akhtar, T.I. Khan, A. Ali Shah, Electrodeposition of Ni-Fe₂O₃ nanocomposite coating on steel, *Surf. Coatings Technol.* 235 (2013) 691–698.
24. R.S. Kate, H.M. Pathan, R. Kalubarme, B.B. Kale, R.J. Deokate, Spray pyrolysis: Approaches for nanostructured metal oxide films in energy storage application, *J. Energy Storage.* 54 (2022).
25. I.B. and E. Valatka, Water-Based Electrophoretic Deposition of Ternary Cobalt-Nickel-Iron Oxides on AISI304 Stainless Steel for Oxygen Evolution, (2022).
26. A. Hajizadeh, T. Shahalizade, R. Riahifar, M.S. Yaghmaee, B. Raissi, S. Gholam, A. Aghaei, S. Rahimisheikh, A.S. Ghazvini, Electrophoretic deposition as a fabrication method for Li-ion battery electrodes and separators – A review, *J. Power Sources.* 535 (2022).
27. M.S.S.M. Meiabadi, A. Kazerooni, M. Moradi, M.J. Torkamany, Laser assisted joining of St12 to polycarbonate: Experimental study and numerical simulation, *Optik (Stuttg.)* 208 (2020) 164151.

28. M. Honarpisheh, E. Haghghat, M. Kotobi, Investigation of residual stress and mechanical properties of equal channel angular rolled St12 strips, *Proc. Inst. Mech. Eng. Part L J. Mater. Des. Appl.* 232 (2018) 841–851.
29. S.A. Hosseini, T. Shahrabi, B. Ramezanzadeh, I. Mohammadi, Nigella sativa extract phytochemicals: Effective green/bio-active anti-corrosion agent for steel protection in saline media, *Ind. Crops Prod.* 202 (2023) 116952.
30. S. Mojallal, H. Mohammadzadeh, A. Aghaeinejad-Meybodi, R. Jafari, Effect of NiO–NiCr₂O₄ nano-oxides on the microstructural, mechanical and corrosion properties of Ni-coated carbon steel, *Int. J. Miner. Metall. Mater.* 27 (2023) 1299–1310.
31. G. Maheshwaran, C. Selvi, R. Kaliammal, M. Ramesh Prabhu, M. Krishna Kumar, S. Sudhahar, Exploration of Cr₂O₃-NiO nanocomposite as a superior electrode material for supercapacitor applications, *Mater. Lett.* 300 (2021) 130191.
32. B. Janani, A. Syed, A.M. Thomas, S. Al-Rashed, L.L. Raju, S.S. Khan, Designing spinel NiCr₂O₄ loaded Bi₂O₃ semiconductor hybrid for mitigating the charge recombination and tuned band gap for enhanced white light photocatalysis and antibacterial applications, *J. Alloys Compd.* 865 (2021) 158735.
33. M. Enhessari, A. Salehabadi, S. Khanahmadzadeh, K. Arkat, J. Nouri, Modified Sol-Gel Processing of NiCr₂O₄ Nanoparticles; Structural Analysis and Optical Band Gap, *High Temp. Mater. Process.* 36 (2017) 121–125.
34. N.A. Noshahi, K. Nadeem, M. Kamran, Role of Mn doping on magnetic properties of multiferroic NiCr₂O₄ nanoparticles, *Ceram. Int.* 47 (2021) 10643–10649.
35. N.M. Deraz, Synthesis and characterization of nano-sized nickel aluminate spinel crystals, *Int. J. Electrochem. Sci.* 8 (2013) 5203–5212.
36. S. Zhou, X. Dai, H. Zheng, Microstructure and wear resistance of Fe-based WC coating by multi-track overlapping laser induction hybrid rapid cladding, *Opt. Laser Technol.* 44 (2012) 190–197.
37. Y. Wang, X. Zhao, E. Hao, Z. Bu, Y. An, H. Zhou, J. Chen, High temperature induced “glaze” layer formed in HVOF-sprayed NiCrWMoCuCBFe coating and its wear reduction mechanism, *Friction.* 10 (2022) 1424–1438.
38. C.T. Kunioshi, O. V. Correa, L. V. Ramanathan, High temperature oxidation and erosion-oxidation behaviour of HVOF sprayed Ni-20Cr, WC-20Cr-7/Ni and Cr₃C₂-Ni-20Cr coatings, *Surf. Eng.* 22 (2006) 121–127.
39. V. Greshta, D. Tkach, E. Sotnikov, D. Pavlenko, O. Klymov, Studying and designing improved coatings for Labyrinth seals of Gas-Turbine engine turbines, *Eastern-European J. Enterp. Technol.* 4 (2018) 56–63.
40. N. Jiang, Y. Liu, X. Yu, H. Zhang, M. Wang, Corrosion resistance of nickel-phosphorus/nano-ZnO composite multilayer coating electrodeposited on carbon steel in acidic chloride environments, *Int. J. Electrochem. Sci.* 15 (2020) 5520–5528.
41. M. Mahmoudi, K. Raeissi, F. Karimzadeh, M.A. Golozar, A study on corrosion behavior of graphene oxide coating produced on stainless steel by electrophoretic deposition, *Surf. Coatings Technol.* 372 (2019) 327–342.
42. D. V Ribeiro, J.C.C. Abrantes, Application of electrochemical impedance spectroscopy (EIS) to monitor the corrosion of reinforced concrete : A new approach, *Constr. Build. Mater.* 111 (2016) 98–104.
43. M. Golabadi, M. Aliofkhaezai, M. Toorani, A.S. Rouhaghdam, Evaluation of La containing PEO pretreatment on protective performance of epoxy coating on magnesium, *Prog. Org. Coatings.* 105 (2017) 258–266.
44. M.M. Khalaf, H.M. Abd El-Lateef, Corrosion protection of mild steel by coating with TiO₂ thin films co-doped with NiO and ZrO₂ in acidic chloride environments, *Mater. Chem. Phys.* 177 (2016) 250–265.